Intratumoral Gold Nanoparticle-Enhanced CT Imaging: An in Vivo Investigation of Biodistribution and Retention*

Rossana Terracciano, Marc L. Sprouse, Dennis Wang, Sara Ricchetti, Matteo Hirsch, Nicola Ferrante, E. Brian Butler, Danilo Demarchi, Alessandro Grattoni and Carly S. Filgueira

***Abstract*— This study aims to evaluate the in vivo distribution of Gold Nanoparticles (GNPs) at different time points after intratumoral (IT) injection, exploiting their properties as contrast agents for Computed Tomography (CT). GNPs approximately 40 nm in diameter were synthesized with a surface plasmon peak at ~530 nm, capped with Bovine Serum Albumin (BSA) to improve colloidal stability, and characterized with standard methods. CT phantom imaging was performed to quantify X-ray attenuation as a function of GNP concentration and surface functionalization and to determine the appropriate particle dose for *in vivo* studies. Concentrated GNPs were intratumorally (IT) injected into Lewis Lung Carcinoma (LLC) solid tumors grown on the right flank of 6-week old female C57BL/6 mice. Ten days post-injection, follow up CT imaging was performed to assess the distribution and retention of the particles in the tumor. Using the CT attenuation quantification, images for each timepoint were segmented, and 3D volumes rendered, to conduct biodistribution analyses. The successful retention and permanence of the GNPs into the solid tumor after ten days suggests the significance of GNPs as a potential theranostic agent.**

I. Introduction

Non-small cell lung cancer (NSCLC) ranks among the most common type of lung cancer, accounting for ~85% of all lung cancer diagnoses, with 5-year cause-specific survival rates ranging from 13% to 32% and local failure rates of 42% to 49% when treated with conventional radiotherapy alone [1]. The engagement to reduce the radiation dose and damage to healthy tissues without losing efficacy in cancer therapy have focused the research on exploiting gold nanoparticle (GNP) properties in enhancing radiation effects via physical, chemical, and biological interactions with ionizing radiation [2]. However, challenges concerning in vivo efficacy still limit the clinical translation of GNP radiosensitizers mainly due to the lack of colloidal stability, clearance, and possible long-term toxicity [3]. Therefore, the ability to predict and determine GNP in vivo biodistribution will provide further information about the preferred uptake pathways for achieving precise dose deposition as well as a better understanding of mechanisms behind radiosensitization [4]. To quantify the biodistribution of GNPs within cells and tissue, several imaging techniques can be employed due to the physical properties of GNPs that allow them to act as imaging agents [5], [6]. This study focuses on Computed Tomography (CT) as an imaging modality to provide insight into the GNP local biodistribution in Lewis Lung Carcinoma (LLC) tumor-bearing mice based on CT attenuation levels. CT is an inexpensive diagnostic imaging system routinely used in practice with a high capability of deeply tissue permeation and density resolution which allows for 3-dimensional (3D) reconstructions of X-ray images. CT contrast agents are commonly administered to improve the contrast among tissues with similar or lower attenuation values by increasing the signal-to-noise ratio without additional radiation doses to the patient. Nevertheless, different drawbacks in the use of iodine-based contrast agents such as renal toxicity, deficiency in the targeting process, and insufficient circulation time as well as amplification in DNA damage during CT scans, restrict their application [7].

Several studies confirm GNPs as excellent contrast agents for CT imaging and multimodalities [8]–[10]. So far, CT image-guided cancer treatments using radio-enhancing GNPs has not been thoroughly investigated in preclinical NSCLC models. The main contribution of this study is to give a better understanding of the in vivo IT distribution and retention of citrate-capped and BSA-capped GNPs using CT imaging.

II. Experimental

A. GNPs Synthesis and characterization

Multi-faceted GNPs (Figure 1A) are synthesized using an adapted protocol by Turkevich et al. [11] to tune the particle size to a value of approximately 40 nm. Briefly, 1 g of gold chloride ($AuCl_3$, purity > 99.99%) is added to 100 mL of Milli-Q water and filtered through a 0.22 μm nylon filter, and 1 g of citric acid ($C_6H_8O_7$) was dissolved in 100 mL of Milli-Q under stirring.

Respectively, 4.8 mL of the 1% (w/v) citric acid solution and 7 mL of 1% (w/v) gold chloride premade reagents are added to 600 mL of boiling Milli-Q water. The synthesis is

*Research supported by the Simmons Foundation, Houston Methodist Research Institute (CF), and Golfers Against Cancer.

R.T. is with the Department of Nanomedicine, Houston Methodist Research Institute, TX, & Dept. of Electronics, Politecnico di Torino, Italy (email: rterracciano@houstonmethodist.org).

E.B.B. is with the Department of Radiation Oncology, Houston Methodist Research Institute, TX. D.D. is with the Dept. of Electronics, Politecnico di Torino, Italy.

M.S., D.W., S.R., M.H., N.F. are with the Department of Nanomedicine, Houston Methodist Research Institute, TX.

A.G. is with the Department of Nanomedicine, Department of Radiation Oncology and Department of Surgery Houston Methodist Research Institute, TX.

C.S.F. is with the Department of Nanomedicine and Department of Cardiovascular Surgery, Houston Methodist Research Institute, TX, (phone: 713-441-1996; email: csfilgueira@houstonmethodist.org)

complete when the color has changed from black to dark red.

The GNPs are characterized with UV-Vis Spectroscopy and electron microscopy (SEM, TEM). Dynamic Light Scattering (DLS) was used to rapidly and qualitatively size the particles and obtain a polydispersity index (PDI). Zeta Potential was also measured (Malvern).

The resulting particles yielded a surface plasmon peak at ~530 nm with a hydrodynamic diameter of 43.89 ± 15.45 nm (Figure 1B). The particle diameter extracted from SEM and TEM images is 39.1 ± 15.0 nm, which is in accordance with the value obtained with DLS (< 11% error). The particle solutions yield Z-potentials of -40.0 ± 6.0 mV.

B. BSA capping and characterization

The GNP surface is then modified by passive absorption of Bovine Serum Albumin (BSA) to increase colloidal stability and biocompatibility. To perform BSA-capping on the GNP surface, lyophilized BSA in a concentration of 2% (w/v) is added to the solution of colloidal gold already prepared and characterized. The mixture is stirred vigorously until complete dissolution of BSA. The absorption of BSA on the particle surface is evaluated by analyzing the UV-Vis spectrum of the solution. A positive passivation of the particles is confirmed by a red-shift in the gold SPR peak at 535 nm (Figure 1b) and the presence of a BSA absorption peak at 280 nm.

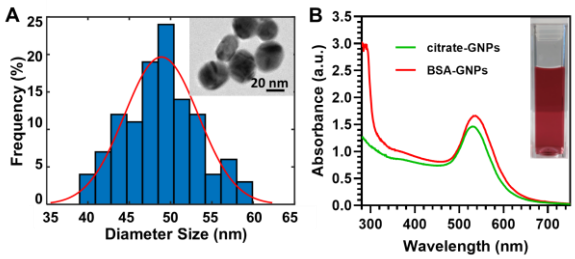

Figure 1. Size distribution (n>100) and TEM image of citrate-GNPs (A). Average particle size: 39.1 ± 15.0 nm. Absorbance spectra of citrate-capped GNPs and BSA-GNPs with absorbance maxima occurring at 530nm and 535nm, respectively (B).

C. CT phantom imaging

In order to prepare the samples for clinical CT phantom imaging, GNP solutions in concentrations ranging from 0 to 10mg/mL are aliquoted in 100 µL tubes and scanned with a Siemens Inveon High-Resolution CT to assess the CT contrast properties (Figure 2). The phantom experiment was carried out using CT parameters with slice thickness of 105 µm, in plane resolution of 105 µm, tube voltage at 80 kV, tube current at 500 µA, exposure time of 240 ms, and by placing the samples directly on the animal bed.

X-ray attenuation intensity was determined in Hounsfield unit (HU) by processing the digital CT images (DICOM files) using 3DSlicer and selecting a 3D reconstructed region of interest (ROI) for each sample and then recording the mean attenuation value and plotting as a function of gold and/or iodine concentration in mg/mL.

As expected, an increase of CT attenuation occurred when the mass concentration of the GNPs increased. Both citrate-GNPs and BSA-GNPs absorb more X-rays than Omnipaque350 (a standard iodine-based CT contrast agent) as shown in Figure 3. The range of CT values for LLC-LUC solid tumor 8 days after cell inoculation is included in the graph for comparison.

D. In vivo CT imaging

High-resolution CT imaging is then exploited to compare the biodistribution of citrate and BSA-capped GNPs in a LLC murine model of NSCLC. *In vivo* imaging experiments were performed using six-week-old female C57/BL6 mice, purchased from Taconic Bioscence (Rensselaer, NY, USA).

The mice received an injection of $2x10^6$ LLC cells in the right flank subcutaneously once their weight reached an average of 18.4 g. After approximately 10 days post-injection, the volumes of tumor nodules appeared spherical and 100 mm^3 in volume. The mice were anesthetized using isoflurane, and 100 µL of citrate or BSA-capped GNPs were injected IT (3.5 mg/mL of gold). CT images pre-injection were recorded as a baseline for the biodistribution analysis. All the CT imaging was performed using a Siemens Inveon Multi-Modality (MM) System controlled with the Inveon Acquisition Workplace (IAW). In vivo experiment was carried out using CT parameters with slice thickness of 103.25 µm, in plane resolution of 103.25 µm, tube voltage at 80 kV, tube current at 500 µA, and exposure time of 240 ms.

The mice were imaged at different time intervals (day 0 pre-injection, day 0 post-injection, day 3 post-injection, day 6 post-injection, day 9 post-injection, and day 10 post-injection). The CT images were acquired and reconstructed with 3DSlicer software.

III. Data Analysis

Figure 4A shows the 3D renderings of three significant timepoints during the ten day post-injection time period. Although both citrate and BSA-capped GNPs exhibited excellent biocompatibility and sustained retention post IT injection, the citrate-GNPs were observed to stably cluster *in situ* over the ten days, while the BSA-GNPs were less likely to locally agglomerate within the tumor (Figure 4B, Figure 4C). Therefore, the BSA helps to facilitate the biodistribution of the GNPs in the tumor area, preventing the formation of clusters.

This evidence is also supported by Figure 5, which shows the differences in particle distribution volume within the tumor tissue. On day 0, the 3D reconstructed volume of the citrate-GNPs from the attenuation values extracted from the CT images is four times smaller than those created by the BSA-GNPs injection. 72h after particle injection, both the citrate and BSA-capped GNPs follow the same constant trend in volume until the tenth day.

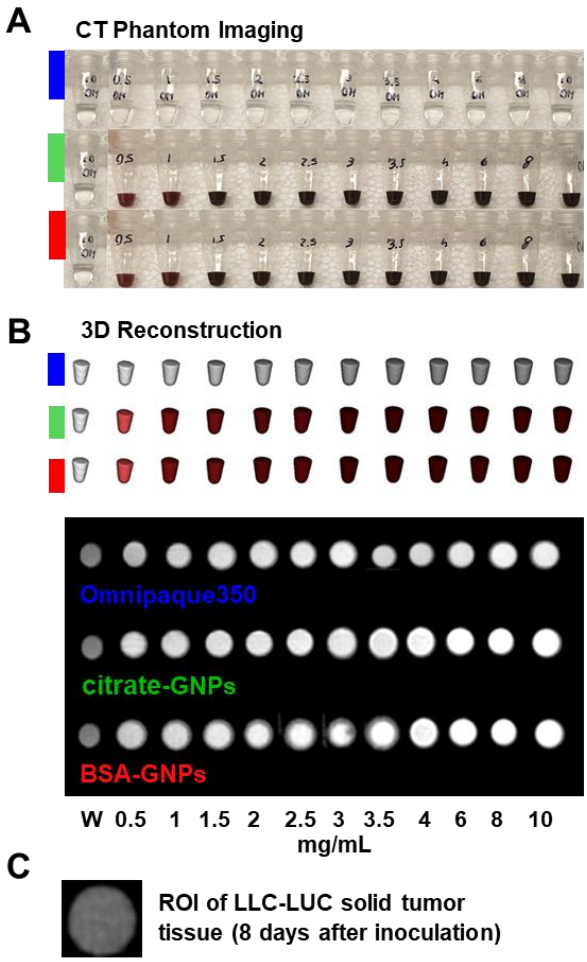

Figure 2. CT Contrast Proprieties of ~40 nm citrate and BSA-capped GNPs Compared with those of Omnipaque350. Photos of the phantom dilution series from 0 (water) to 10 mg/mL concentrations for Omnipaque350 (blue), citrate-GNPs (green), and 2% (w/v) BSA-capped GNPs (red) (A). Representative 3D volume rendered CT images and sample phantom images from Siemens Inveon High Resolution CT scanner (B). For a better understanding and comparison is reported a ROI of the LLC tumor 8 days after cell inoculation and immediately before GNP injection (C).

In order to better understand the IT biodistribution pattern over time and eventually the clearance of the particles, we quantified the contrast in several organs at different time points. Figure 6 represents the CT values of attenuation (HU) of the heart, brain, kidneys, liver, intestine, tumor and bladder, extracted from circular ROIs selected on the CT images at the different time points after administration of citrate and BSA-capped GNPs. Due to the presence of clusters in the case of injections of citrate-GNPs, the analysis is divided into sub-measures for the tumor:

1. GNPs Intra-cluster (IC) to indicate the ROI inside the tumor and inside the cluster of GNPs
2. GNPs Extra-cluster (EC) to indicate the ROI inside the tumor and outside the cluster of GNPs.

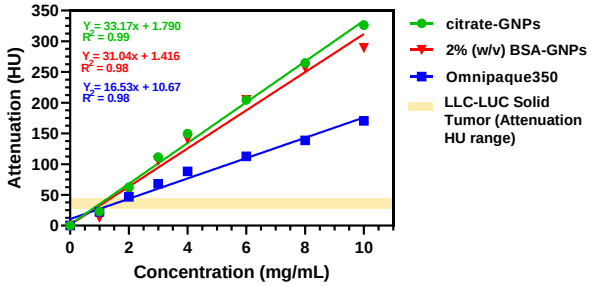

Figure 3. X-ray attenuation changes in Hounsfield Units (HU) versus concentration for citrate and BSA-capped GNPs compared with those of Omnipaque350. Data are reported in terms of mean value of the 3D reconstructed voxel attenuations and standard deviations. To trace the thresholds for choosing the optimal concentration to inject, the LLC tumor tissue density range 8 days after cell inoculation and immediately before GNPs injection is reported (yellow range).

As seen in Figure 6A, citrate-GNPs clusters are well enclosed in the tumor and remain there even after 10 days. The extra-cluster tumor area doesn't show the presence of particles over time. The absence of citrate-GNPs over time in this area indicates a biodistribution capability of the particles under the limits of detection. The CT attenuation results here suggest that the citrate-GNPs are not excreted in 10 days. This conclusion is further deduced because when compared to the baseline, no visible attenuation increments are distinguishable in other organs over time.

Conversely, the CT results from the images of BSA-GNPs-injected mice confirm contrast enhancement in the tumor ROI at the first time point (immediately after injection of BSA-GNP) with attenuation values of 354 HU, ~8% higher than the baseline (325 HU). Furthermore, the contrast remains stable over the subsequent 3 days, while at day 10, comes back to baseline levels. Despite the high accumulation in the intestine and partial changes in the other organs (heart, brain, kidneys, liver and bladder), the results suggest that the particles could be excreted after 10 days. Heart, brain, kidneys and liver all returned to baseline levels after 10 days, while the CT signals of the intestine increased gradually, indicating bile excretion of the particles. Accumulation in the bladder is still present after 10 days. This could indicate a nearly complete excretion of the particles from the body after 10 days.

Despite their good biodistribution capabilities, a point of discussion is the lack of *in vivo* contrast enhancement of the BSA-GNPs when compared to the citrate-GNPs (~50% and ~8%, respectively). It becomes clear that a better and more immediate distribution in the tumor environment compromises CT contrast properties. Hence, the importance of calibrating the CT attenuation of the GNPs before *in vivo* injection for tracing a safe threshold and leveraging the CT-contrast proprieties of the particles.

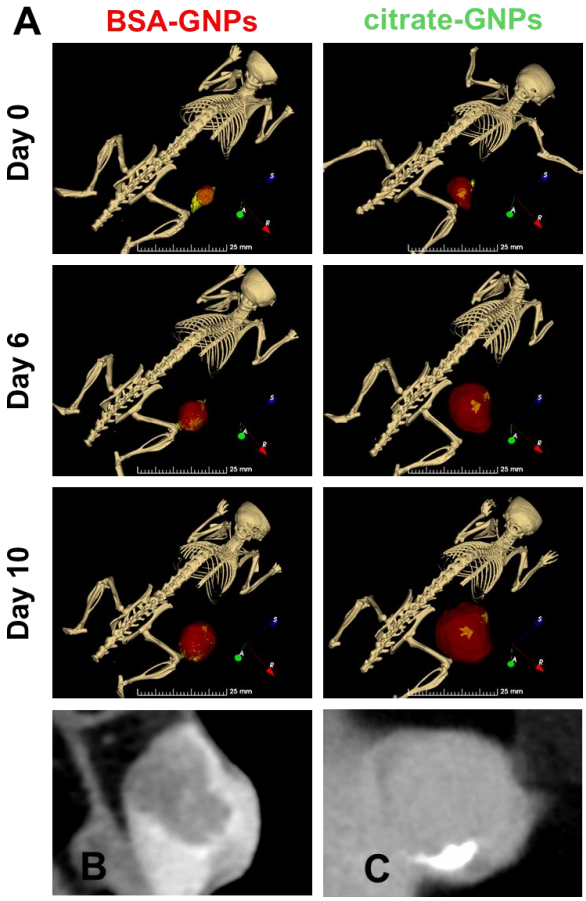

Figure 4. Representative 3D volumes rendered CT images at day 0 immediately after IT injections of 100µL BSA-capped GNPs and citrate-GNPs solutions, day 6 and day 10 after IT injection. All the images are displayed at window width of 1500 HU and window level 700 to cover bone, metal and tumor tissue attenuations. The voxel size of the images is 105µm. The grayscale look up table is then shown in a more natural-like color and GNPs are displayed in yellow (A). CT slices of mice bearing tumors, cropped specifically in the tumor region immediately after BSA-GNPs injection (B) and citrate GNPs (C), where the clustering process is more evident.

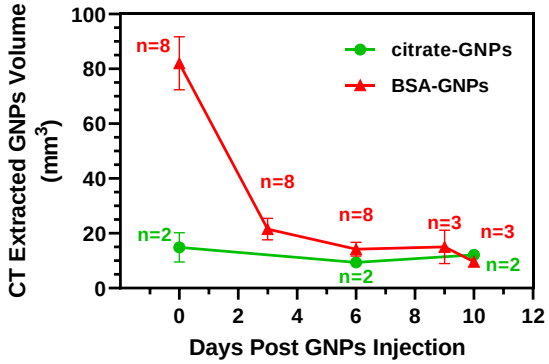

Figure 5. 3D reconstructed volumes (mm^3) of the GNPs from the attenuation values extracted from the CT images over the imaging timepoints.

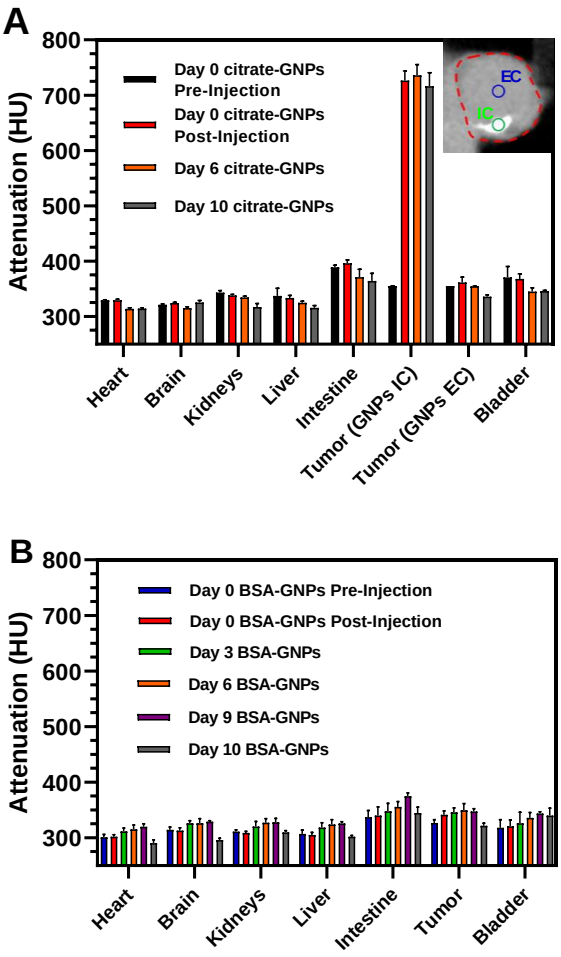

Figure 6. The CT attenuation values (HU) of various organs at different time points after administration of (A) citrate-GNPs and (B) BSA-GNPs. The analysis for citrate-GNPs divides the tumor ROIs in GNPs Intracluster (IC) and GNPs Extracluster (EC).

IV. Conclusion

In conclusion, the permanence of the GNPs into the tumor after ten days suggests the significance of GNPs as a potential theranostic agent. Further, the more homogeneous and uniform IT distribution of the BSA-GNPs may offer further advantages for surface passivation.

Animal Experiment

All experiments conducted on mice were approved by the Institutional Animal Care and Use Committee (IACUC) at Houston Methodist Research Institute and were performed according to the principles of the NIH Guide for the Care and Use of Laboratory Animals, the provisions of the Animal Welfare Act, PHS Animal Welfare Policy, and the policies of the Houston Methodist Research Institute. Housing and care were provided in accordance with the regulations of the Animal Welfare Act and recommendations of the Guide for the Care and Use of Laboratory Animals.

ACKNOWLEDGMENT

Funding support was received from the Simmons Foundation, Houston Methodist Research Institute (CF), and Golfers Against Cancer agencies. We are grateful to Dr. Xukui Wang, the Houston Methodist Research Institute Translational Imaging - PreClinical Imaging (Small Animal) Core, and the Houston Methodist Research Institute Microscopy Core.

REFERENCES

[1] C. J. Miller et al., "Predictors of Distant Failure After Stereotactic Body Radiation Therapy for Stages I to IIA Non–Small-Cell Lung Cancer," Clin. Lung Cancer, vol. 20, no. 1, pp. 37–42, Jan. 2019, doi: 10.1016/j.cllc.2018.09.002.

[2] S. Her, D. A. Jaffray, and C. Allen, "Gold nanoparticles for applications in cancer radiotherapy: Mechanisms and recent advancements," Adv. Drug Deliv. Rev., vol. 109, pp. 84–101, Jan. 2017, doi: 10.1016/j.addr.2015.12.012.

[3] Y. Chen et al., "Gold nanoparticles coated with polysarcosine brushes to enhance their colloidal stability and circulation time in vivo," J. Colloid Interface Sci., vol. 483, pp. 201–210, Dec. 2016, doi: 10.1016/j.jcis.2016.08.038.

[4] S. Rosa, C. Connolly, G. Schettino, K. T. Butterworth, and K. M. Prise, "Biological mechanisms of gold nanoparticle radiosensitization," Cancer Nanotechnol., vol. 8, no. 1, p. 2, Dec. 2017, doi: 10.1186/s12645-017-0026-0.

[5] D. Kim et al., "Label-free high-resolution 3-D imaging of gold nanoparticles inside live cells using optical diffraction tomography," Methods, vol. 136, pp. 160–167, Mar. 2018, doi: 10.1016/j.ymeth.2017.07.008.

[6] R. Meir et al., "Nanomedicine for Cancer Immunotherapy: Tracking Cancer-Specific T-Cells in Vivo with Gold Nanoparticles and CT Imaging," ACS Nano, vol. 9, no. 6, pp. 6363–6372, Jun. 2015, doi: 10.1021/acsnano.5b01939.

[7] M. M. Mahan and A. L. Doiron, "Gold Nanoparticles as X-Ray, CT, and Multimodal Imaging Contrast Agents: Formulation, Targeting, and Methodology," Journal of Nanomaterials, 2018. https://www.hindawi.com/journals/jnm/2018/5837276/ (accessed Mar. 23, 2020).

[8] R. Cheheltani et al., "Tunable, biodegradable gold nanoparticles as contrast agents for computed tomography and photoacoustic imaging," Biomaterials, vol. 102, pp. 87–97, Sep. 2016, doi: 10.1016/j.biomaterials.2016.06.015.

[9] M. F. Ghaziyani et al., "Anti-CD24 bio Modified PEGylated Gold Nanoparticles as Targeted Computed Tomography Contrast Agent," Adv. Pharm. Bull., vol. 8, no. 4, pp. 599–607, Nov. 2018, doi: 10.15171/apb.2018.068.

[10] Y. C. Dong et al., "Effect of Gold Nanoparticle Size on Their Properties as Contrast Agents for Computed Tomography," Sci. Rep., vol. 9, no. 1, pp. 1–13, Oct. 2019, doi: 10.1038/s41598-019-50332-8.

[11] J. Turkevich, P. C. Stevenson, and J. Hillier, "The Formation of Colloidal Gold," J. Phys. Chem., vol. 57, no. 7, pp. 670–673, Jul. 1953, doi: 10.1021/j150508a015.